Ballistic Limit Determination in Impacts on Multimaterial Laminated Targets

K. N. KREYENHAGEN,* M. H. WAGNER,* J. J. PIECHOCKI,† AND R. L. BJORK‡
Shock Hydrodynamics, Inc., Sherman Oaks, Calif.

Two-dimensional numerical analyses have been performed of projectile impacts at 15,000–20,000 fps into finite laminated targets consisting of plastic layers backed by aluminum substrates. These analyses used the SHAPE code, with a hydrodynamic-elastic-plastic distortional model. Three solutions are discussed. The first illustrates phenomena occurring during impacts just under the perforation threshold. Results showing the time-resolved development of rear surface bulging are compared with dynamic observations of parallel experiments. Good agreement is obtained. The second and third solutions show conditions leading to perforation. Using a generalized plastic strain criterion, two failure modes are identified. Petalling tends to occur where the plastic front layer of the target is relatively thick and the failure criterion is first exceeded on the back surface near the axis. Plugging occurs in thinner targets when the failure criterion is first exceeded at an off-axis location on the plastic-substrate interface. Through use of SHAPE and this failure criterion, predictions can be made as to whether a given impact will perforate a given multilayered target.

I Introduction

IMPACTS at hypervelocities into thick or semi-infinite targets have been examined in the past by two-dimensional, axisymmetric numerical solutions, utilizing both purely hydrodynamic models and hydrodynamic-elastic-plastic models.[1–4]

Impacts into thin targets, where complete perforation easily occurs, have also been numerically treated. In such cases, behind-target debris characteristics are of considerable interest in designing meteoroid bumpers. Reference 5 discusses results of a numerical study of such impacts.

For many design problems, the most important hypervelocity impact conditions are those which are near the ballistic limit of a target, i.e., the threshold where a target is just barely perforated by an impact. In these cases, the early stages of impact are characterized by extreme pressures and, hence, are primarily hydrodynamic in nature. The final stages, in which the back of the target deforms and subsequently comes to rest (or is just barely perforated), are clearly dominated by the elastic-plastic properties of the material.

In this paper, hypervelocity impacts against targets consisting of a layer of plastic backed by a metal substrate are examined, and a technique for predicting whether or not a given impact will perforate such a target is demonstrated.

The numerical solutions which are illustrated herein were obtained through use of the two-dimensional SHAPE program. SHAPE, an acronym for Shock Hydrodynamic and Plastic Elastic, utilizes either a Particle-in-Cell (PIC)[6] or an Eulerian[7] code for analysis of the initial, essentially hydrodynamic processes. The solution is subsequently transformed to a Lagrangian computational method for treatment of the late-stage, strength-dominated response. The Lagrangian formulation which is used is based upon the model of Wilkins.[8] The SHAPE program is described in Ref. 9.

II Impact Response of Multilayered Targets

To illustrate the physical processes involved in impact on a multilayered target, a numerical solution of such a problem will be used. Figure 1 shows the impact conditions. Additional inputs required for the numerical solution are the material properties and a failure criterion. For the plastic material, the pressure (P) was prescribed by an equation of state of the form

$$P = A(\mu) + G\eta e \tag{1}$$

where $A(\mu) = 0.172\mu + 0.327\mu^2 + 0.777\mu^3$, and where e is the internal energy per unit original volume, η is the relative density, and μ is the compression. A value of 0.504 is assigned to the Grüneisen constant G. The properties of the plastic were further described by the specification of the yield strength = 0.001 Mb and the shear modulus = 0.047 Mb.

The 6061-T6 aluminum was described by a Los Alamos-type equation of state[10]

$$P = (A + Be + Ce^2)/(e_0 + e) \tag{2}$$

where $A = 1.187\mu + 0.763\mu^2$, $B = 3.45 + 1.545\mu + 0.964\mu^2$, $C = 0.434 + 0.549\mu$, and $e_0 = 1.5$. The aluminum was further specified by the normal density = 2.7 g/cm^3 and the shear modulus = 0.274 Mb. The increase in strength as a result of work hardening was accounted for by the empirically-derived relationships $Y = 0.0029 + 0.026\bar{\epsilon}_p - 0.122\bar{\epsilon}_p$ (when $\bar{\epsilon}_p \leq 0.106$) and $Y = 0.0043$ (when $\bar{\epsilon}_p > 0.106$). In these relationships, Y is the yield strength (in Mb) and $\bar{\epsilon}_p$ denotes the generalized plastic strain. The latter quantity is defined by Hill[11] as

$$\bar{\epsilon}_p = \int d\bar{\epsilon}_p \tag{3}$$

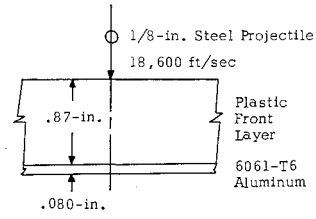

Fig. 1 Impact conditions for numerical solution.

Presented as Paper 69-356 at the AIAA Hypervelocity Impact Conference, Cincinnati, Ohio, April 30–May 2, 1969; submitted May 28, 1969; revision received May 18, 1970. This research was sponsored by U. S. Air Force Space and Missile Systems Organization (AFSC).

*Senior Scientific Staff.
† Senior Scientific Staff. Member AIAA.
‡ Now Consultant, Northridge, Calif.

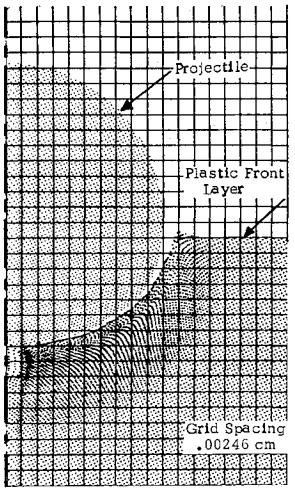

Fig. 2 Mass positions at 0.24 μsec.

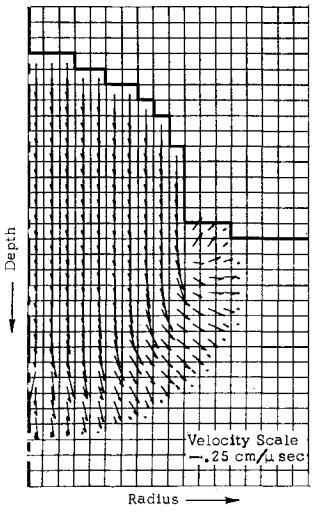

Fig. 3 Particle velocities at 0.24 μsec.

where

$$d\bar{\epsilon}_p = (\tfrac{2}{3} d\epsilon_{ij}{}^p d\epsilon_{ij}{}^p)^{1/2}$$

and $\epsilon_{ij}{}^p$ are the tensor components of plastic strain.

Failure of a bilaminate target of the type shown in Fig. 1 occurs when the substrate layer is ruptured. To provide a means in the numerical solution which would determine if substrate rupture would occur, a failure criterion was specified for the aluminum. This criterion establishes a maximum level of the generalized plastic strain, defined by Eq. (3), which an element of material may suffer without failure. Generalized plastic strain is a monotonically increasing function, which is increased by any type of plastic deformation that the material suffers. The critical value of $\bar{\epsilon}_p$ can be derived from conventional tension failure test data. For 6061-T6 aluminum, $\bar{\epsilon}_p \approx 0.3$ in the case of equibiaxial loading, which is approximately true for the problems of interest here.

Figures 2 and 3 show spatial plots of mass position and particle velocity at 0.24μsec after impact. This is during the hydrodynamic PIC portion of the solution. The field of view shown in these figures corresponds to the computational region during the early stages. It does not include all of the target thickness, but is confined to the active region near the impact. As the shocked region enlarges, the computational region is periodically expanded. In Fig. 2, it is seen that the plastic target material is being compressed by the oncoming projectile. Deformation of the relatively stiff steel projectile is less marked. The velocity vectors in Fig. 3 represent the average velocity of the mass in each

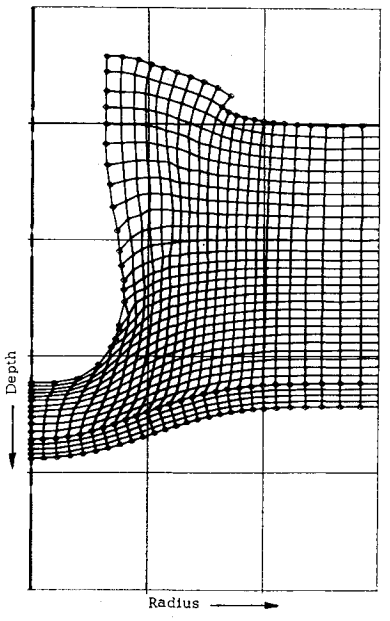

Fig. 5 Lagrangian net at 27.4 μsec.

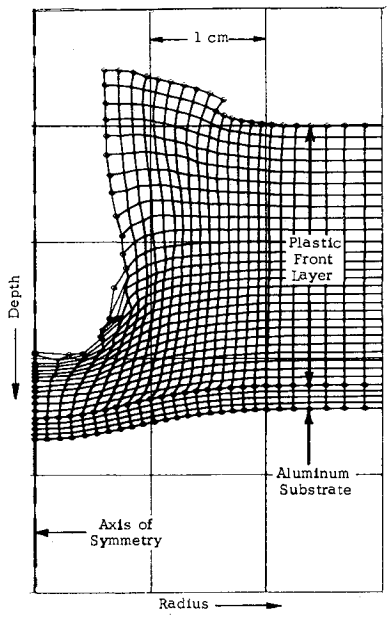

Fig. 4 Lagrangian net at 17.5 μsec.

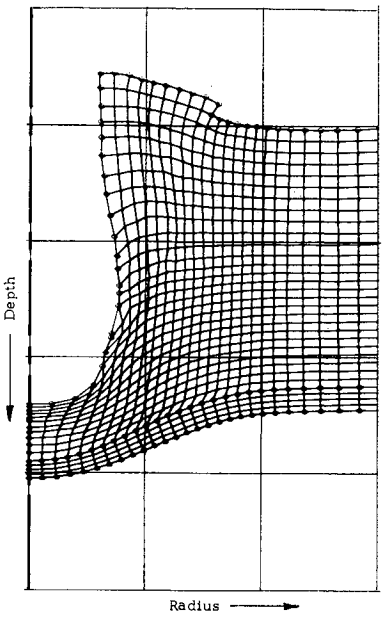

Fig. 6 Lagrangian net at 53.9 μsec.

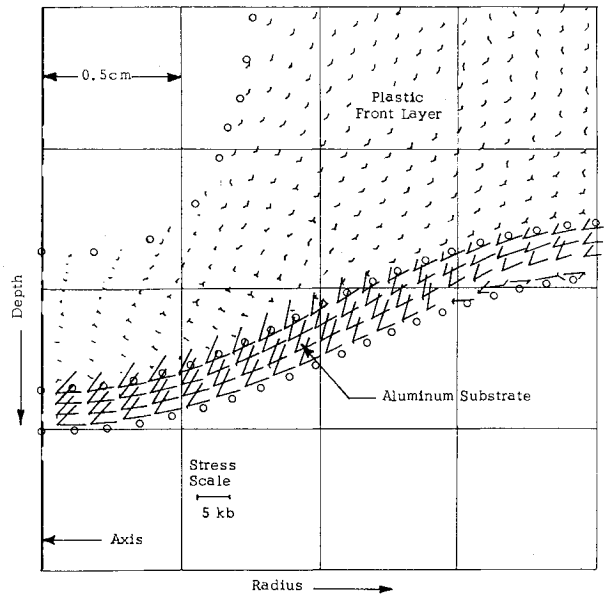

Fig. 7 Principal stress field at 37.9 μsec.

computational cell. Lateral flow of target material is beginning to occur, because of the proximity of the surface and to geometric dispersion in the target.

The PIC solution was continued until the shock front reached the plastic-aluminum interface, which occurred at 4.7 μsec after impact. At this point, the PIC computational grid was overlayed by a rectangular Lagrangian grid. Parameters in each PIC cell at 4.7 μsec were appropriately repartitioned among the new Lagrangian cells, and the solution was continued in the Lagrangian computational mode. From this point on, material strength was explicitly included in the solution.

As the shock wave impinges upon the substrate, it delivers an impulse to that layer, thereby transferring the axial momentum of the projectile to the substrate. The subsequent response of the substrate acts to transfer the axial momentum laterally to adjacent parts of the target.

Figures 4–6 show the distortion of the Lagrangian net at 17.5, 27.4, and 53.9 μsec (the end of the solution). The hole in the plastic continues to increase in depth. The substrate develops a large bulge in response to the impulse imparted to it by the shock-wave system.

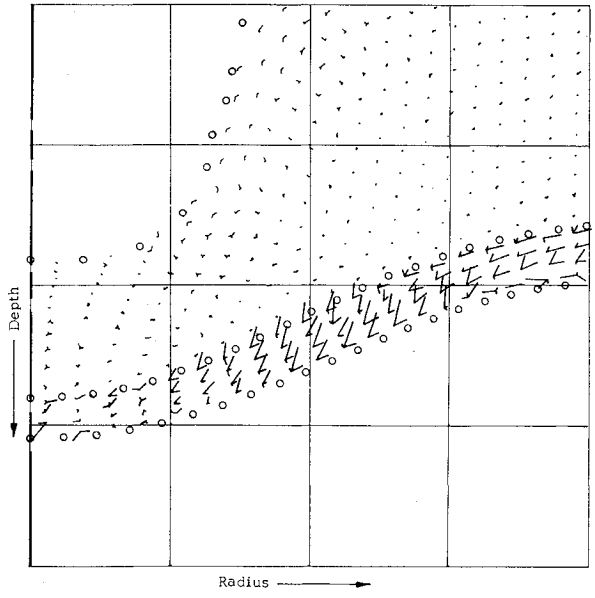

Fig. 8 Principal stress field at 53.9 μsec.

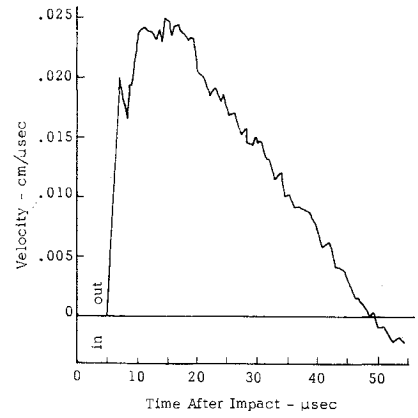

Fig. 9 Velocity of crown of substrate bulge vs time after impact.

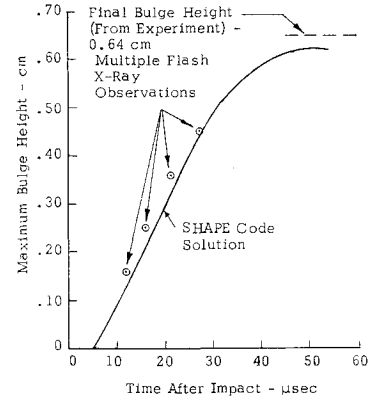

Fig. 10 Bulge height vs time after impact.

Since perforation, if it occurs, will be the result of rupture of the substrate, it is of interest to observe the development of the principal stress field in the bulging substrate. Figures 7 and 8 are enlarged views of this portion of the stress field at 37.9 and 53.9 μsec. The two-orthogonal principal directions in the r-y plane are identified. In each principal direction, the magnitude of the corresponding principal stress is plotted. The third principal direction is always in the azimuthal (θ) direction. Its magnitude is plotted along a diagonal bisecting the principal directions in the r-y plane. As a sign convention, vectors having downward components denote compression, while those having upward components indicate tension.

In Figures 7 and 8, the only significant principal stresses are the tensile stresses parallel to the substrate surface and the diagonally-plotted tensile hoop stresses. Stresses normal to the substrate surface are largely eliminated by the presence of the free surface. Thus the substrate bulge is essentially in a condition of membrane tension.

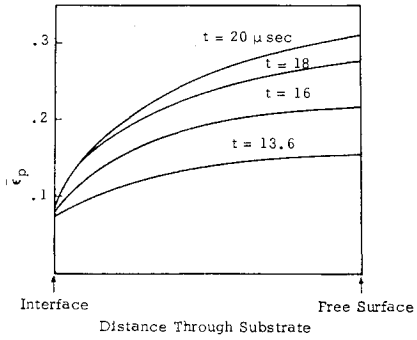

Fig. 11 Generalized plastic strain in substrate along axis at several times after impact.

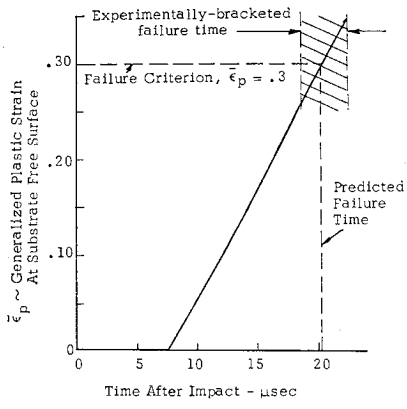

Fig. 12 Generalized plastic strain near bulge crown vs time.

As the substrate bulge enlarges, the membrane tension acts as the mechanism for lateral transfer of axial momentum to adjacent portions of the target. As the substrate motion is thus gradually arrested, stress relief occurs, as is evident near the crown in Fig. 8.

Figure 9 shows the velocity profile at the substrate bulge apex. Outward motion of the bulge apex stops at 48 μsec, followed by some inward motion, or recovery due to elastic effects. Figure 10 shows corresponding bulge height-time profiles, indicating that the bulge displacement reaches a maximum value of 0.63 cm at about 50 μsec.

Experimental data have been independently obtained for this impact condition by investigators at IITRI.[12] These data consist of a sequence of flash radiographs showing the development of the substrate bulge displacement, plus post-test measurements of the residual bulge height. The experimental data points are plotted on Fig. 10 and are seen to correspond very closely with the numerical solution.

III Prediction of Failure in Multilayered Targets

In the preceding problem, the substrate came to rest without rupture. If subjected to a somewhat more energetic impact, it is evident that rupture would have occurred. A numerical solution of such a case serves to illustrate the use of the generalized plastic strain criterion for predicting rupture.

The early time response of the target was similar to the previous numerical example, and will not be repeated here. The substrate absorbed axial momentum from the impact, subsequently causing bulging. The generalized plastic strain in each cell was monitored as the solution advanced in time. The largest values were found along the centerline of the bulge. Figure 11 shows the generalized plastic strain in the row of computational cells immediately adjacent to the axis at several times after impact. The values are always greatest at the rear free surface, i.e., the crown of the bulge. The critical value of $\bar{\epsilon}_p = 0.3$ is exceeded in that cell at 20 μsec, indicating that rupture starts at that time. Figure 12 shows $\bar{\epsilon}_p$ in the apex cell vs time from the solution. Experimental observations of this impact have also been made by IITRI.[12] From sequential flash radiographs of the substrate rear surface, the time of initial rupture of the surface

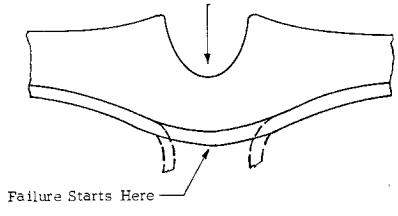

Fig. 13 Petalling-type failure.

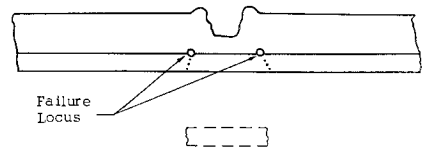

Fig. 14 Plugging-type failure.

was bracketed between the values shown in Fig. 12. The numerical prediction of failure time falls within this bracket.

In this experiment and in others where failure first occurred at the crown of the bulge, the substrate subsequently ruptured by petalling, as illustrated in Fig. 13.

Where the front layer or layers in a multilayered target are not sufficiently thick to permit geometric dispersion of the shock-wave system, the impulse delivered to the substrate will be concentrated in a small area, and failure may occur by plugging as illustrated by Fig. 14. Figure 15 shows the Lagrangian net from the numerical solution of an impact which resulted in plugging. This net shows the distortion of the substrate at the time the $\bar{\epsilon}_p = 0.3$ failure criterion was first exceeded. This occurred in two off-axis cells on the inside surface of the substrate (the interface with the plastic layer). If an annular crack propagated through the target at the radius of the outermost failed cell, a hole of about 0.45-cm radius would be formed. In an experimental impact under these conditions, the hole formed had a 0.48-cm radius.

Figure 16 shows $\bar{\epsilon}_p$ in the row of cells through the substrate along the centerline and along the 7th row of cells. In both instances $\bar{\epsilon}_p$ is greater on the inner surface of the substrate. However, the $\bar{\epsilon}_p = 0.3$ criterion is first exceeded in the off-axis cell.

IV Summary

It is seen that hypervelocity impact upon a multilayered target produces a strong shock-wave system in the front layer or layers. As this shock system propagates through the front layers, it expands geometrically. When the shock reaches the substrate layer, it delivers an impulse to that layer, which in effect then becomes a momentum trap. In order to survive the impact, the substrate layer must dis-

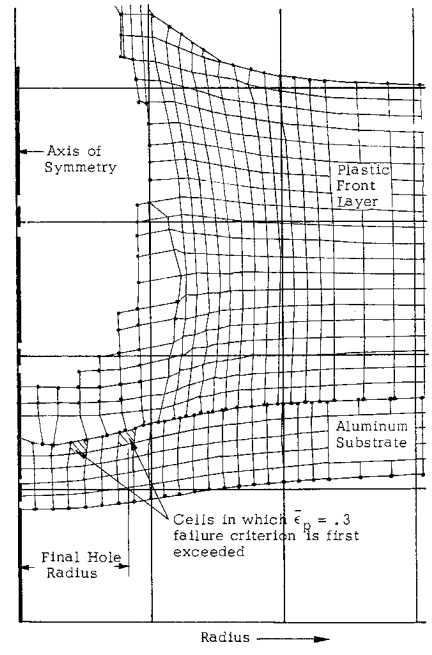

Fig. 15 Labrangian net at 12.9 μsec showing location of cells where failure criterion is exceeded to produce plugging-type failure.

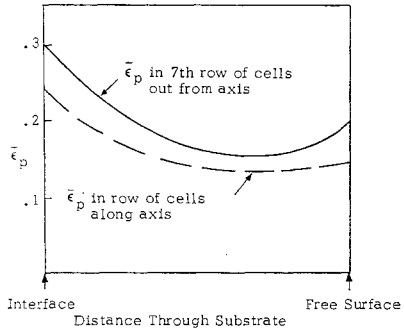

Fig. 16 Generalized plastic strain at 12.9 μsec along axis and along 7th row of cells.

tribute the axial momentum laterally to adjacent portions of the target.

Failure of the substrate occurs by petalling or by plugging, or a combination of these. Petalling-type rupture occurs when the front layers of a target are sufficiently thick to disperse the impulse delivered to the substrate over a relatively large area. A broad bulge in the substrate is thus formed. Failure first occurs on the rear surface near the crown when the material there reaches a critical value of generalized plastic strain.

Plugging-type failure occurs when the front layers are not thick enough to permit geometric dispersion of the shock-wave system, such that a concentrated impulse is delivered to the substrate. Failure by this mode first occurs on an off-axis locus on the inner surface of the substrate. As in the petalling case, failure by plugging is initiated when a material element first suffers a generalized plastic strain exceeding the given criterion.

References

[1] Bjork, R. L., "Effects of a Meteoroid Impact on Steel and Aluminum in Space," *Proceedings of the Tenth International Astronautical Congress*, Springer-Verlag, 1959, p. 505.

[2] Bjork, R. L., "Review of Physical Processes in Hypervelocity Impact and Penetration," *Proceedings of the 6th Symposium on Hypervelocity Impact*, Firestone Tire & Rubber Co., Vol. 2, Pt 1, 1963, pp. 1–58.

[3] Walsh, J. M. and Tillotson, J. H., "Hydrodynamics of Hypervelocity Impact," *Proceedings of the 6th Symposium on Hypervelocity Impact*, Firestone Tire & Rubber Co., Vol. 2, Pt 1, 1963, pp. 59–104.

[4] Riney, T. D., "Visco-Plastic Solution of Hypervelocity Impact Cratering Phenomenon," *Proceedings of the 6th Symposium on Hypervelocity Impact*, Firestone Tire & Rubber Co., Vol. 2, Pt 1, 1963, pp. 105–140.

[5] Rosenblatt, M., Kreyenhagen, K. N., and Romine, W. D., "Numerical Studies of Ejecta Characteristics Behind Thin Plates," *AIAA Journal*, Vol. 8, No. 6, June 1970, pp. 1005–1011.

[6] Bjork, R. L., Brooks, N. B., and Papetti, R., "A Numerical Technique for Solution of Multidimension Hydrodynamic Problems," RM2628-PR, 1963, The Rand Corp., Santa Monica, Calif.

[7] Read, H. E., "Hardening Technology Studies II, STRIDE, A Three-Dimensional Code," BSD-TR-67-191, Aug. 1967, Space and Missile Systems Organization, Norton Air Force Base, Calif.

[8] Wilkins, M. L., "Calculation of Elastic-Plastic Flow," UCRL-7322, April 1963, Univ. of California Lawrence Radiation Lab., Livermore, Calif.

[9] Brooks, N. B. and Lansdale, R. L., "Hardening Technology Studies III, SHAPE-II Code," SAMSO-TR-68-69, Jan. 1968, Space and Missile Systems Organization, Norton Air Force Base, Calif.

[10] Osborne, R. K., personal communication, 1960, Los Alamos Scientific Lab.

[11] Hill, R., *The Mathematical Theory of Plasticity*, 1st ed., Oxford, New York, 1950, p. 30.

[12] Nagoaka, H. H., personal communication, 1968, Illinois Institute of Technology Research Institute.